PHILOSOPHICAL TRANSACTIONS A

rsta.royalsocietypublishing.org

Research

Article submitted to journal

Subject Areas:
Statistical Physics

Keywords:
Nonlinear Physics, Path Integral method, Stochastic Process, Transitions induced by noise, Mean first passage time

Author for correspondence:
Enrique Tirapegui
e-mail: etirapeg@gmail.com

Supporting Information. Numerical Path Integral calculation of the probability function and exit time: An application to non gradient drift forces.

Fernando Mora, Pierre Coullet, Sergio Rica and Enrique Tirapegui

The current supporting information contains details on the numerical scheme for the simulations of stochastic differential equations. The algorithm is complemented with examples for a couple of time independent Langevin forces as well as two time dependent forces. Additionally we have included the results of computation for the probability distribution function for two one-dimensional systems (pitchfork and subcritical) by the three methods mentioned on the main paper. We conclude with details on the numerical work regarding a couple of two- dimensional systems, namely, a general Hopf bifurcation and a bistable codimension 2 model.

This supporting information also contains some movies: "TimeDependentFig2.mov" that shows the evolution of the snapshots of Fig 2 of the main paper "2DModel.mov" that shows the iterations of the path integral scheme till reaches the stationary state solution for the bistable 2D model (3.5)-(3.6) and "ExitTime.mov" that shows the loss of probability of an initial probability distribution located at one attractor.

THE ROYAL SOCIETY PUBLISHING

1. Stochastic differential equations: The Runge-Kutta Algorithm

A one dimensional stochastic differential equation (SDE) is an equation of the form (see Eq. (1) of the main paper)

$$\dot{x} = f(x,t) + \sqrt{\eta}\,\xi(t). \tag{1.1}$$

in which η is the noise intensity and $\xi(t)$ is a white Gaussian δ-correlated noise such that

$$\langle \xi(t) \rangle = 0 \quad \text{and} \quad \langle \xi(t_1)\xi(t_2) \rangle = \delta(t_1 - t_2),$$

These equations can normally be solved only numerically by using standard methods of solution of Stochastic Differential Equations (SDE) [1]. For the numerical findings in the main paper we use a first order Runge Kutta algorithm [2], creating a set of realizations or trajectories and later calculating the PDF over this set. To be more explicit, equation (1.1) is written in the so-called Ito form as

$$dx_t = f(x_t)\,dt + \sqrt{\eta}\,dW_t \tag{1.2}$$

in which $dW_t = \xi(t)\,dt$ is the Wiener Process [3]. Let $X_0 = x_0$ an initial condition and $[0,T]$ the interval over which (1.2) must be integrated. The numerical solution for a trajectory of (1.2) by the RK algorithm is then approximated by the Markov Chain X_n, in which the index n denotes the time dependence, defined recursively as

$$X_{n+1} = X_n + \frac{1}{2}(K_1 + K_2), \tag{1.3}$$

for $n = 0, 1, ..., N$, and in which

$$\begin{aligned} K_1 &= \Delta t f(X_n) + \sqrt{\eta}\,(\Delta W_n - S_{n_1}\Delta t), \\ K_2 &= \Delta t f(X_n + K_1) + \sqrt{\eta}\,(\Delta W_n + S_{n_2}\Delta t), \end{aligned}$$

with $S_{n_{1,2}} = \pm 1$, each alternative chosen with probability 1/2, $\Delta t = \frac{T}{N}$ and the ΔW_n are independent and identically distributed normal random variables with mean 0 and variance Δt. The explicit form of the term ΔW_n is given by

$$\Delta W_n = \sqrt{\Delta t}\,Z_n$$

with Z_n a normal random variable. In order to generate the Z_n we use the Box-Muller-Wiener algorithm [1] as follows: Let U_1 and U_2 be a pair of independent random variables that are uniformly distributed in the interval $(0,1]$, and compute

$$Z = \sqrt{-2\,\log(U_1)}\cos(2\pi U_2),$$

then, Z is a normal random variable.

(a) Simulation of SDE for a time-independent Langevin force

(i) Numerical simulation for $\dot{x} = \mu x - x^3 + \sqrt{\eta}\,\xi(t)$.

The RK scheme described in the previous section (equation (1.3) can be directly applied for the integration of a time-independent Langevin equation. Fig. 1 shows six trajectories or realizations obtained by integrating the SDE $\dot{x} = \mu x - x^3 + \sqrt{\eta}\,\xi(t)$ using the described RK algorithm as well as the deterministic solution (black dotted curve) of the noiseless equation.

(ii) Numerical simulation for $\dot{x} = \mu + x^2 - \alpha x^3 + \sqrt{\eta}\,\xi(t)$

Similarly, Fig. 2 shows five trajectories or realizations obtained by integrating the SDE $\dot{x} = \mu + x^2 - \alpha x^3 + \sqrt{\eta}\,\xi(t)$ using the RK algorithm.

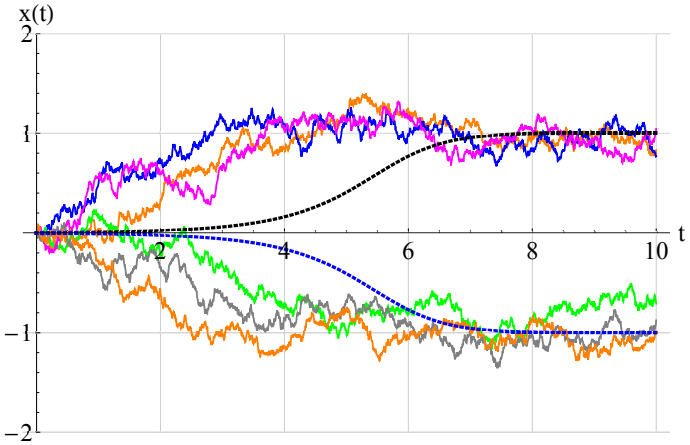

Figure 1. A set of 6 realizations for the SDE $\dot{x} = \mu x - x^3 + \sqrt{\eta}\,\xi(t)$ representing a Pitchfork Bifurcation with initial condition $x(0) = x_0 = 0.003$ for the deterministic upper branch and $x_0 = -0.003$ for the lower branch. In the simulation we set $\epsilon = 1.0$, and the amplitude of the noise is $\eta = 0.09$. The black and blue dotted curves are the deterministic solutions when $\eta = 0$. For solving the stochastic equation we discretize the time interval [tmin, tmax] = [0, 10] in the RK algorithm by setting a time step dt = 0.005.

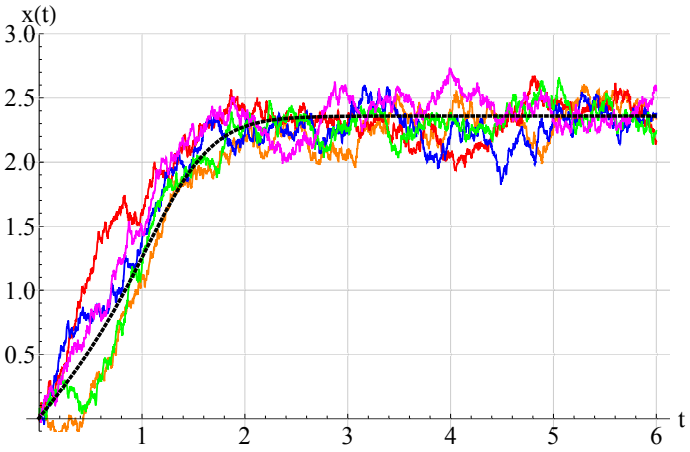

Figure 2. A set of 5 realizations for the SDE $\dot{x} = \epsilon + x^2 - \alpha x^3 + \sqrt{\eta}\,\xi(t)$ with initial condition $x(0) = x_0 = 0.005$. In the simulation we set $\epsilon = 1.0$, $\alpha = 0.5$ and the amplitude of the noise is $\eta = 0.2$. The black dotted curve is the deterministic solution with $\eta = 0$. For solving the stochastic equation we discretize the time interval [tmin, tmax] = [0, 6] in the RK algorithm by setting a time step dt = 0.002.

(b) Simulation of SDE for a time-dependent Langevin force

The scope of the RK algorithm is not limited to time independent Langevin forces, it does indeed work correctly for time-dependent cases as well.

(i) Numerical simulation of $\dot{x} = at + x^2 + \sqrt{\eta}\,\xi(t)$.

In this section we show the results obtained by applying the scheme based on equation (1.3) for the Langevin time-dependent stochastic differential equation

$$\dot{x} = at + x^2 + \sqrt{\eta}\,\xi(t). \tag{1.4}$$

This model was suggested by Dorodnitsyn [6] in the mid forties and more recently by Pomeau and collaborators [7] to model the forecasting of catastrophic events. In equation (1.5) the factor at plays the role of the bifurcation parameter in a saddle node bifurcation. If $at < 0$ one has a quasi-static situation, that is, if $a \ll 1$, then the solution is $x \approx \pm\sqrt{-at}$, however as soon as $at > 0$ these solutions become complex numbers. For the sake of clearness, set $\alpha = \eta = 0$, then equation (1.5) is of Riccati's type and it can be integrated by the substitution

$$x(t) = -\frac{y'(t)}{y(t)},$$

where $y(t)$ satisfies the linear Airy equation $y''(t) + (at)y(t) = 0$, so that $y(t) = c_1 Ai(-a^{1/3}t) + c_2 Bi(-a^{1/3}t)$. For simplicity, take $c_2 = 0$ then, $x(t) \approx -\sqrt{-at}$ as $t \to -\infty$, more important, the first zero, $a^{1/3}t \approx 2.338$, of the Airy function, $Ai(-a^{1/3}t) = 0$, represents a finite-time singularity of the physical variable $x(t) \approx 1/(t_* - t)$. In figure (Fig. 3) it can be seen a simulation of the deterministic and its stochastic counterpart for equation (1.4).

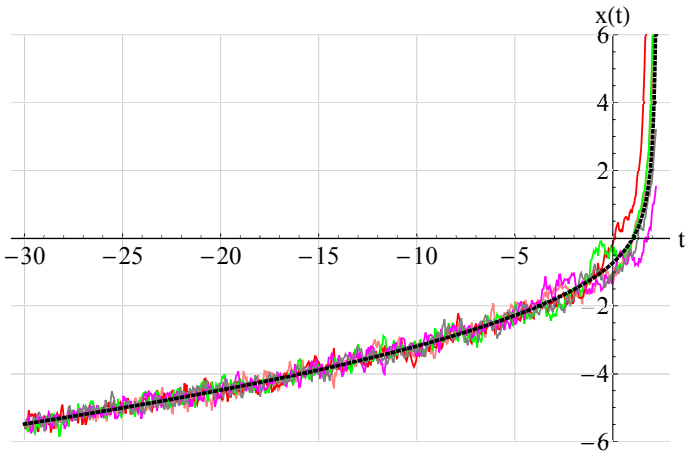

Figure 3. A set of 5 realizations for the SDE $\dot{x} = at + x^2 + \sqrt{\eta}\,\xi(t)$ with initial condition $x(-30) = x_0 = -5.47$. In the simulation we set $a = 1.0$ and the amplitude of the noise is $\eta = 0.7$. The black dotted curve is the deterministic solution with $\eta = 0$. For solving the stochastic equation we discretize the time interval [tmin, tmax] = [-30, 2.2] in the RK algorithm by setting a time step dt = 0.05.

(ii) Numerical simulation of $\dot{x} = at + x^2 - \alpha x^3 + \sqrt{\eta}\,\xi(t)$.

Previous model predicts a finite time singularity that may be annoying in the numerical study of the probability density functions a s a function of time. Therefore we include the parameter α is to avoid the occurrence of this singularity. In Ref. [7] the presence of noise plays an important role, as the statistical properties of precursors may give information about the existence or not of a catastrophe.

In this line we have performed numerical simulations applying previous scheme to equation

$$\dot{x} = at + x^2 - \alpha x^3 + \sqrt{\eta}\,\xi(t). \tag{1.5}$$

As done in previous sections, we integrate the stochastic differential equation using the first order Runge-Kutta method (1.3). Fig. 4 shows six different numerical realizations of equation (1.5), showing that the transition or catastrophe time is quite unpredictable (in the same plot is shown the deterministic trajectory when $\eta = 0$).

The above scheme is the core in which we can calculate the probability distribution function in the corresponding section on the time-independent Langevin force, by generating 6000

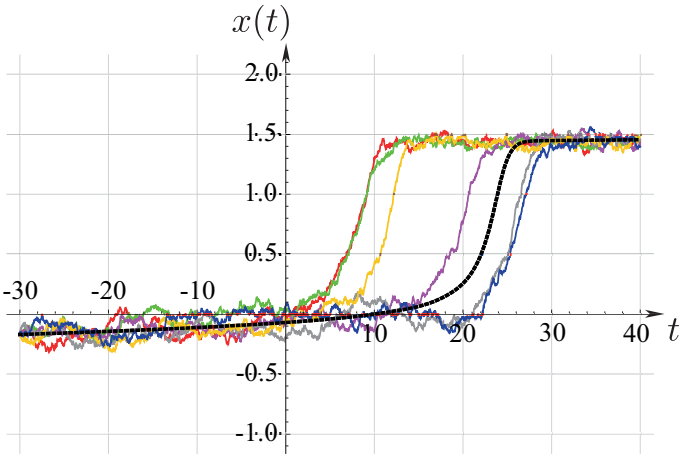

Figure 4. Numerical simulations of equation (1.5) for 6 different realizations, with parameters $a = 10^{-3}$, $\alpha = 0.7$, $\eta = 0.005$. The black segmented curve is the solution for the noiseless equation by the standard Runge-Kutta algorithm and trajectory's curves are calculated solutions by simulation of the SDE employing the RK scheme. The time step is $\Delta t = 0.03$. over a time interval $[-30, 40]$.

realizations. Then having computed the realizations a frequency histogram is constructed and the probability distribution function is obtained by normalizing the histogram, shown in Fig. 2 of the main paper.

2. Probability distribution function and MET in various 1-D situations.

Two general cases were studied in one dimension to test the numerics: a pitchfork and a subcritical bifurcation. We compute the PDF by calculating the probability distribution function after generating a large number of realisations of the SDE (1.1). We compare it, by computing numerically a discretised version of the path integral kernel (Eqn. (3.7) of the main paper), and solving the eigenvalue problem (Eqn. (3.10) of the main paper) to find the stationary probability.

As a first example let's consider the codimension 1 pitchfork bifurcation :

$$f_1(x,t) = \mu x - x^3. \tag{2.1}$$

This Langevin force follows a symmetric double-well potential, $f_1(x) = -V'(x)$, with $V(x) = -\mu x^2/2 + x^4/4$. This system has two stable fixed points at $x = \pm\sqrt{\mu}$ (attractors) and one unstable fixed point at $x = 0$. A second example is the Langevin force for the subcritical bifurcation:

$$f_2(x,t) = \epsilon + x^2 - \alpha x^3. \tag{2.2}$$

This is also a potential case with $V(x) = -\epsilon x - x^3/3 + \alpha x^4/4$, however is a codimension 2 bifurcation, the transition points $\epsilon = 0$ and $\epsilon = -\frac{4}{27\alpha^2}$, representing a saddle node bifurcation. As is well known, this saddle node is defined by the disappearing of two equilibrium points (one stable and another unstable). For $-\frac{4}{27\alpha^2} \leq \epsilon \leq 0$, the system possesses bi-stability, that is there are two stationary stable solutions. In terms of energy, the potential has two stability basins of attraction. These solutions are connected by the remaining unstable solution.

Fig. 5 shows the PDF for the cases of Pitchfork and sub-critical bifurcations. We arrive at the numerical solution via the computation of the PDF calculated from a large number of realizations of the respective SDE by employing the stochastic RK algorithm.

Additionally, for the computation of the stationary probability is employed the path integral kernel (Eqn. (3.5) of the main paper). We compute it by discretising the spatial variables,

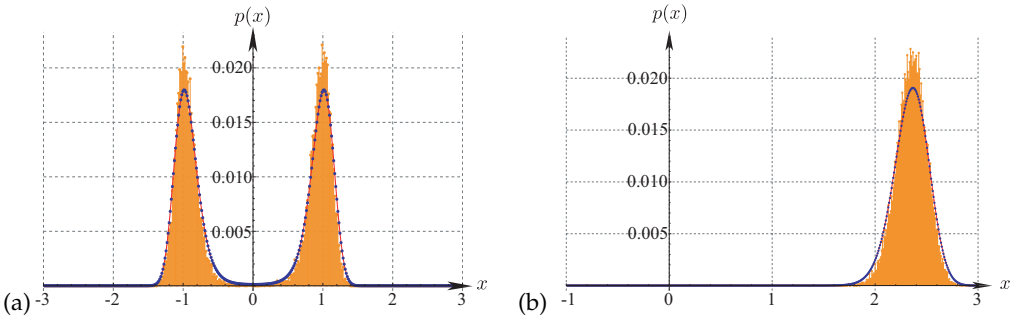

Figure 5. Normalised PDF for the case of a pitchfork bifurcation (2.1) and a subcritical bifurcation (2.2) with noise. Each plot contains an orange bar plot with the normalised PDF, computed from realisations of the respective SDE by the RK scheme. The continuous red line represents the path integral computation, that is $\boldsymbol{p}^{eq}$ (defined through eqn. (3.10) of the main paper)), and the blue dots show the result of the exact stationary probability ($p_{st} \sim e^{-V(x)/\eta}$, see eqn. (2.6) of the main paper). The kernel spatial discretisation is $N = 400$ and $N = 500$ points respectively. (a) Pitchfork bifurcation (2.1) with $\mu = 1$ (hence he attractors are located at $x = \pm 1$), $\eta = 0.1$, $dt = 0.25$ and 18000 realisations. (b) Subcritical bifurcation, (2.2), with $\epsilon = 1.0$, $\alpha = 0.5$ (attractor is located at $x = 2.36$). The stochastic simulation parameters are $\eta = 0.2$ and 18000 realisations.

restricting the domain of the x variable to the interval $[-3, 3]$ and dividing it into 400 points and $[-1, 3]$ and 500 points for the second bifurcation. The discretised kernel, a 400×400 matrix, allows us to compute the equilibrium probability after the Eigenvalue problem (eqn. (3.10) of the main paper). Finally, we compare both numerical solutions with the exact stationary probability, which always exists in one-dimensional cases.

To compute the mean exit time we make use of a known result in one dimension [5] known as Dynkin's formula, which allows the computation of MET over a potential barrier from an attractor located at a point x_A on the left well up to a saddle point x_C:

$$\tau = \tau(x_A, 0) = \frac{2}{\eta} \int_{x_C}^{x_A} dy\, e^{\frac{2V(y)}{\eta}} \int_{y}^{-\infty} e^{-\frac{2V(z)}{\eta}}\, dz. \tag{2.3}$$

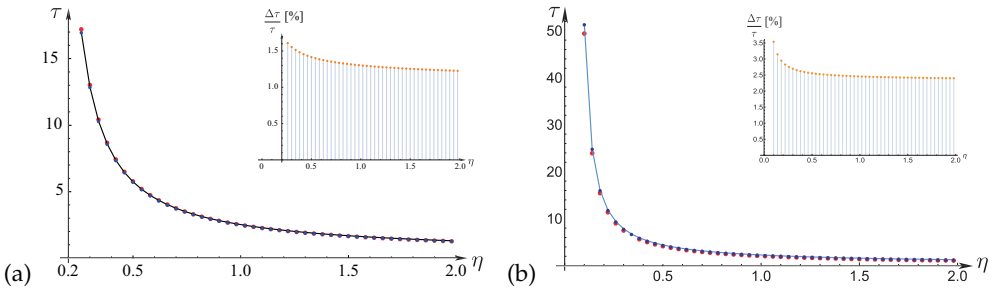

Figure 6. Mean first passage time $\langle \tau(x', 0) \rangle$ as a function of noise intensity η, with an initial probability $p_0(x) = \delta(x - x')$. Continuous line correspond to Dynkin's formula (2.3) and red dots correspond to the path integral method using formula (3.13) of main paper. The insets plot the relative error between both solutions (a) Mean first passage time (MFPT) for the pitchfork bifurcation (2.1) with $\mu = 1$, and an initial trajectory starting at $x' = -1$ vs. noise amplitude η. (b) MFPT as a function of noise intensity η for the sub-critical bifurcation (2.2) with $\epsilon = -0.2$, $\alpha = 0.5$ and an initial trajectory starting at $x' = -0.41$.

The results of computing the Mean Exit Time for the same two previous cases, using Dynkin's formula (2.3) and Path Integral's formula (3.13) in main paper are shown in Fig. (6). It compares both calculations for the cases of the pitchfork (2.1) and subcritical (2.2) bifurcations. Because the mean first passage time depends explicitly on the original probability distribution, for purposes of comparison we have settled the initial probability distribution at the attractors of the specific Langevin force. As we can see, in Figs. 6 (a) and (b), both computations are almost not distinguishable from each other with a relative difference less than few percent.

3. Non-gradient drift forces [9,10].

Stationary solutions of the Fokker-Planck equation satisfies the d-dimensional partial differential equation:

$$\frac{\partial}{\partial x^\mu}\left(f^\mu(\boldsymbol{x},t)P - \frac{\eta}{2}\frac{\partial}{\partial x^\nu}Q^{\mu\nu}P\right) = 0. \tag{3.1}$$

In the limit of small noise, $\eta \ll 1$, the stationary probability is approximated by a WKB like expansion

$$p_{st}(\boldsymbol{x},\eta) = e^{-\frac{1}{\eta}\phi(\boldsymbol{x},\eta)}, \tag{3.2}$$

with $\phi(\boldsymbol{x},\eta) = \phi^{(0)}(\boldsymbol{x}) + \eta\,\phi^{(1)}(\boldsymbol{x}) + \eta^2\,\phi^{(2)}(\boldsymbol{x}) + \ldots$ The zero-order term, $\phi^{(0)}(\boldsymbol{x})$ satisfies a Hamilton-Jacobi equation for $\phi(\boldsymbol{x})$, namely [9,10]:

$$D^{\mu\nu}\frac{\partial\phi^{(0)}}{\partial x^\mu}\frac{\partial\phi^{(0)}}{\partial x^\nu} + f^\mu(\boldsymbol{x})\frac{\partial\phi}{\partial x^\mu} = 0. \tag{3.3}$$

Notice that in the previous Hamilton-Jacobi equation is equivalent to define

$$f^\mu(\boldsymbol{x}) = -D^{\mu\nu}\frac{\partial\phi^{(0)}}{\partial x^\nu} + R^\mu(\boldsymbol{x}),$$

where $R^\mu(\boldsymbol{x})$ a reminder term, together with the orthogonality condition:

$$R^\mu(\boldsymbol{x})\frac{\partial\phi^{(0)}}{\partial x^\mu} \equiv 0.$$

The most probable points are the minimum of $\phi^{(0)}$, hence $\frac{\partial\phi^{(0)}}{\partial x^\nu} = 0$, therefore in this case, though the system reaches equilibrium, the Langevin forces are not null, because $f^\mu(\boldsymbol{x}) = R^\mu(\boldsymbol{x})$.

Though this nonlinear eikonal-like equation (3.3) can be solved in some situations, however, as expected, in most general cases the system does not have a potential gradient over all the phase space. In what if follows we show two examples having simple solutions.

(a) Hopf-bifurcation

Consider the normal form of the Hopf-bifurcation [8]:

$$\dot{A} = A - (1+i\alpha)|A|^2 A, \tag{3.4}$$

for the complex amplitude $A(t) = x(t) + iy(t)$. One readily notices that in this case the potential is the usual "mexican-hat" U(1),

$$\phi^{(0)}(A,\bar{A}) = -|A|^2 + \frac{1}{2}|A|^4,$$

and the reminder term is

$$R = -i\alpha|A|^2 A,$$

which is orthogonal to the potential gradient. Moreover,

$$\dot{A} = -\frac{\partial\phi^{(0)}}{\partial\bar{A}} + R.$$

As noticed by Jauslin [9], the "equilibrium" points, the minima of ϕ, are not stationary as in a usual gradient drift dynamical system. Indeed, looking for the condition $\frac{\partial \phi^{(0)}}{\partial \bar{A}} = \mu A - |A|^2 A = 0$, one gets $A_u = 0$, which is a local maxima, and $|A_s|^2 = 1$, which is a degenerate minima, *i.e.* $A_s = e^{i\delta}$ represents a continuous family of solutions. These solutions do not vanish the drift because $R = -i\alpha A_s$, represents a rotational dynamics:

$$\dot{A}_s(t) = -i\alpha A_s \quad \Leftrightarrow \quad A_s = e^{-i\alpha t}.$$

(b) A two-dimensional bistable system.

Consider the co-dimension 2 model [12] (which is a variation of Maier and Stein's model [11], eqn. (4.2) of main paper):

$$\dot{x} = \mu_1 x - x^3 - \frac{1}{\mu_2}(\mu_1 - \mu_2) y^2 x \tag{3.5}$$

$$\dot{y} = \mu_2 y - y^3 - \left(\frac{\mu_2}{\mu_1} + \nu \frac{\mu_1}{\mu_2}\right) x^2 y \tag{3.6}$$

Because of the polynomial character of the above, one may find a polynomial non-equilibrium potential, subsequently with the property that the asymptotic expansion will eventually close. A solution can be found by setting:

$$\begin{aligned} D &= \begin{pmatrix} 1 & 0 \\ 0 & \nu \end{pmatrix}, \\ \phi^{(0)} &= -\mu_1 x^2 + \frac{1}{2}x^4 + \frac{\mu_1}{\mu_2} x^2 y^2, \\ R &= \begin{pmatrix} xy^2 \\ y\left(\mu_2 - \frac{\mu_2 x^2}{\mu_1} - y^2\right) \end{pmatrix}. \end{aligned} \tag{3.7}$$

The correctness of the above expressions can be readily verified by the interested reader. Finally, we point out that the extreme of $\phi^{(0)}$ corresponds to the points: $(\pm\sqrt{\mu_1}, 0)$ (local minima) and $(0, 0)$. In both cases the drift vanishes exactly at these points.

4. Path-integral numerical computations

.

The results of the path integral computation of previous models and the subsequent comparison with the solution based on the non-equilibrium potential are given in figures 7 and 8. Fig. 7 considers a Hopf bifurcation, which exhibits rotational symmetry in the (x, y) plane. Consequently to compare both solutions we "cut" at a vertical plane which passes through $y = 0$. We show the surface probability distributions of the solution based on the non-equilibrium potential and the resulting one based on the Path Integral Scheme, after 100 iterations (50 Iterations for the case $\eta = 0.07$) for $\eta = 0.5$ and the superposition of the cuts at the plane $y = 0$ for both solutions for three noise intensities.

Fig. 8 shows the surface plot for the case of the bistable model (3.5)-(3.6), which has mirror symmetry through $y = 0$ and $x = 0$ and in which are shown the $3D$ surfaces by both methods for the three noise intensities and with common 120 iterations. The superposition of cuts at $x = 0$ and $y = 0$ are shown as a main result into the paper.

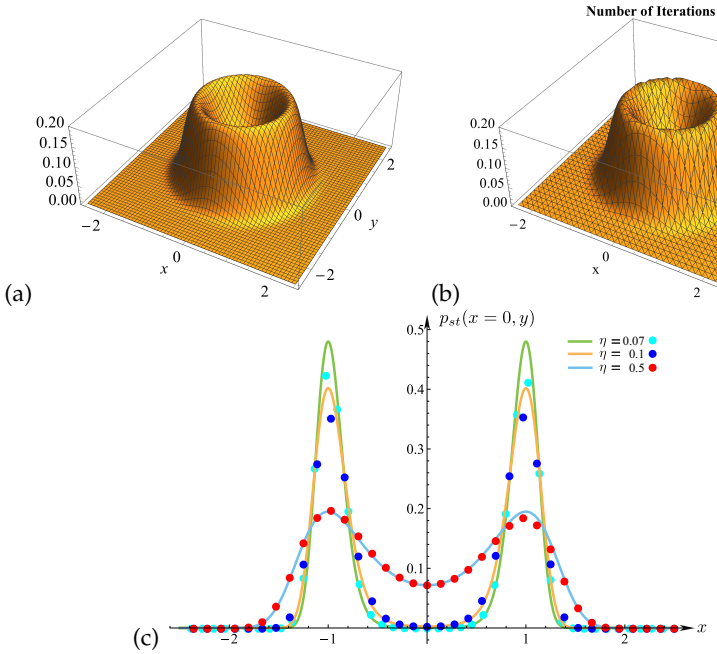

Figure 7. Path Integral solutions and transversal cuts at $y=0$ for model of equation (3.4). The parameters are $\alpha=0.5$, $N=36$ points spatial discretization, 100 iterations for path integral computation when noise $\eta=\{0.1,0.5\}$. (a) Analytic 3D Surface for $\eta=0.5$. (b) Path Integral 3D Surface for $\eta=0.5$. (c) Transversal cuts superimposed at $y=0$ for cases $\eta=\{0.07,0.1,0.5\}$. In the case $\eta=0.07$ the spatial discretization was 44 points and the number of iterations 50.

5. Mean Exit Time

In the following we provide some details of the analysis of the numerical data for the path integral computation of mean exit time. First, the exit time requires the calculation of the probability transition from one attractive fixed point to another. This problem goes through a restriction of the basin of attraction of one stable fixed point. We call this basin of attraction Ω. Therefore one needs to determine the geometry of Ω. In the current case we consider the stable fixed point at $x=-\sqrt{\mu_1}$ and $y=0$, and more important, because of the symmetries, the separatrix of the dynamical system is just the y-axis located at $x=0$, therefore

$$\Omega=\{(x,y)/-\infty<x\leq 0\ \&\ -\infty<y<\infty\}\,.$$

The discretisation restricts the domain to a rectangular domain of 50 points distributed in a physical domain of size $L\times 2L$. For the numerics we need to compute the full discretized normalised kernel, $\mathcal{K}$, for a square domain $2L\times 2L$ that mimics the whole phase space. Next, the full Kernel is restricted up to $\mathcal{K}_\Omega$ (1/4 smaller in size than the full Kernel). As initial condition we consider a Gaussian

$$p_0(x,y)\sim e^{-\frac{1}{2\sigma^2}\left((x+\sqrt{\mu_1})^2+y^2\right)},$$

of width σ located at the aforementioned fixed point.

Then the path integral algorithm :

$$\boldsymbol{p}^\Omega(t+1)=\mathcal{K}_\Omega\boldsymbol{p}^\Omega(t),$$

is ruled as far as desired. At each time step one sums the contribution over Ω to obtain the total probability loss rate:

$$n^\Omega(t)=\left\langle \mathbf{1}_\Omega|\boldsymbol{p}^\Omega(t)\right\rangle, \tag{5.1}$$

as a function of time.

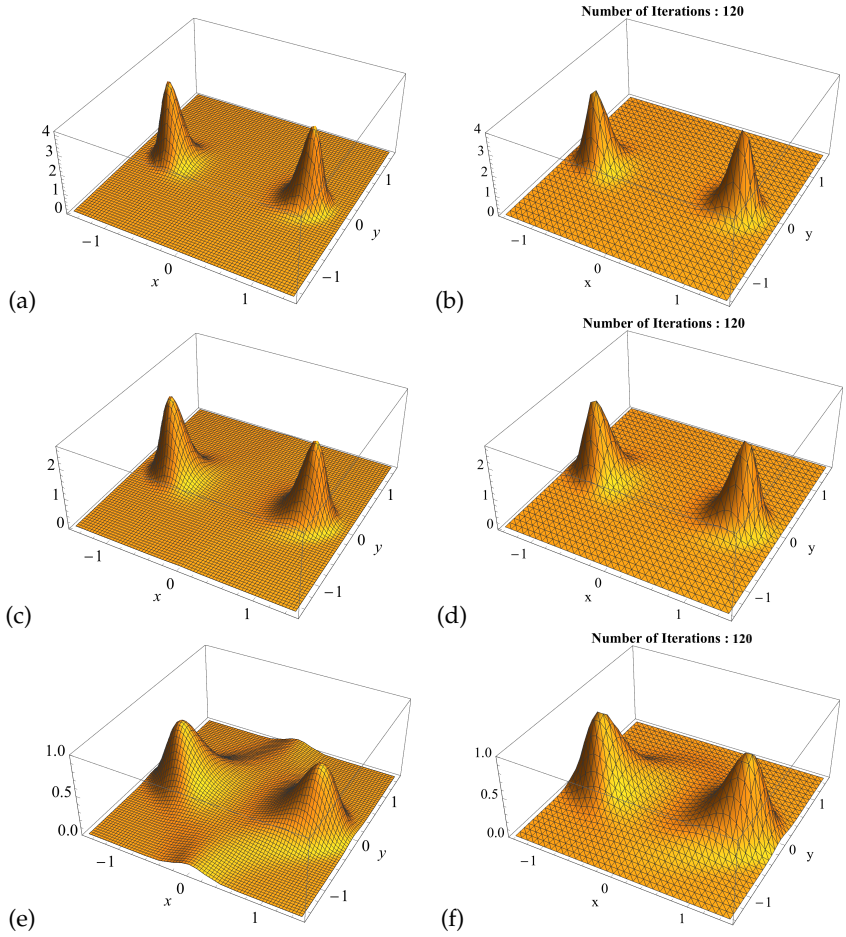

Figure 8. Analytic and Path Integral solutions for Bistable model (3.5)-(3.6) as function of noise. The parameters are $N = 36$ points spatial discretization, 120 iterations for path integral computation, $\mu_1 = 1.0$, $\mu_2 = 0.5$ and $\nu = 1.0$. (a) Analytic, $\eta = 0.07$. (b) Path Integral, $\eta = 0.07$. (c) Analytic, $\eta = 0.1$. (d) Path Integral, $\eta = 0.1$. (e) Analytic, $\eta = 0.25$. (f) Path Integral, $\eta = 0.25$.

Fig. 9-a shows a typical exponential decay of the total probability lost (5.1) as a function of time. As expected $n^{\Omega}(t)$ typically decreases exponentially in time, for instance for the case of Fig. 9-a one fits

$$\hat{n}^{\Omega}(t) = Ae^{-\lambda t}, \text{ with } \quad A = 1.00852 \text{ and } \lambda = 3.901367 \times 10^{-5}.$$

We have estimated the mean exit time in a threefold way:

(i) By using directly formula, $\tau = \epsilon \sum_{t=0}^{\infty} n^{\Omega}(t)$.
This method which works only in the case of moderate run times restrict the computational possibilities to $\eta \gtrsim 0.07$. For instance for $\eta = 0.05$ the total probability has up to a factor of 0.52 in relation to the initial one. To overcome this difficulty we add the following alternative estimates.
(ii) Use an exponential fit and set $\tau = 1/\lambda$.
(iii) Use an exponential fit and integrate $\tau = \int_0^{\infty} \hat{n}^{\Omega}(t)dt$.

Fig. 9-b shows the integration of the fitted exponential behaviour (iii) after 250000 iterations, however, its final value may be estimated after 50000 steps by method (iii). Contrarily one notices that the estimate (ii) is about 0.85% lower than (i) and (iii).

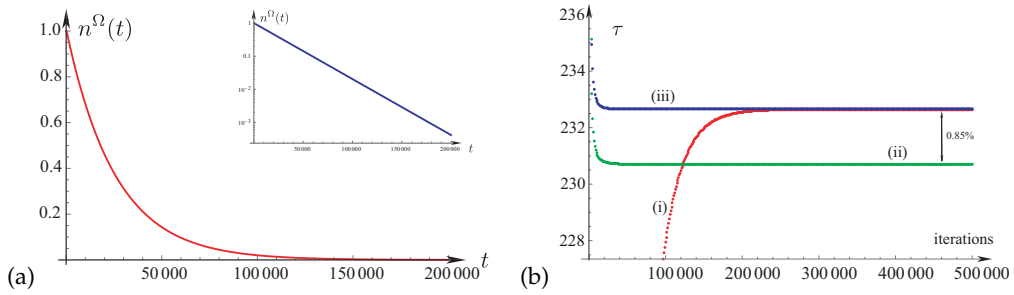

Figure 9. a) The total probability $n^{\Omega}(t)$ in the attraction basin as a function of time. The inset confirms the exponential decaying behavior. Here $\eta = 0.1$, $\sigma = 0.1$, $dx = 0.03$. b) The three estimates as a function of the iteration step. One notices that the estimate (iii) by the coefficient λ is 0.85 % smaller that the other estimates.

The procedure has been repeated for several noise intensities in the range $0.03 \leq \eta \leq 2.5$. Conversely we have run the numerics for two distinct values of L such that the mesh sizes are respectively $dx = 0.03$ ($L = 1.5$) and $dx = 0.06$ ($L = 3$) finding results which do not vary substantially as it can be seen in Fig. 3b of the main paper. Finally we also check the robustness under two different initial configurations.

Fig. 10 shows the dependency of the three estimates as a function of the width σ. One notices that the estimate (i) and (iii) are quite similar and decreases as σ increases. We understand that by the following argument, as the width of the initial probability reaches the separatrix the mean exit time is expected to diminish drastically in the first iterations. On the other hand, the estimate (ii) by the coefficient λ is constant, this is because λ is related to the spectrum of the Kernel $\mathcal{K}_{\Omega}$, something that is intrinsic to stochastic systems and does not depend on the initial condition. Finally for the estimation, we conclude that $\sigma < 0.2$ provides a safe estimation for a localized initial probability.

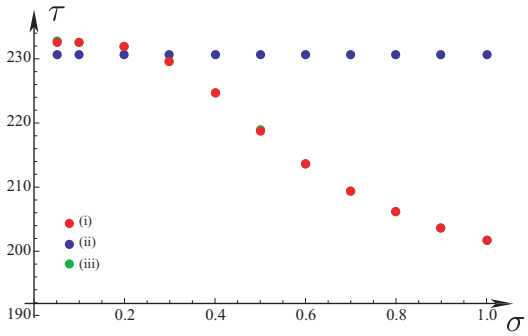

Figure 10. Mean exit time as a function of the initial width of the probability distribution σ. The asymptotic value as $\sigma \to \infty$ is $\tau \to 191.9$ for (i) and (iii), while $\tau \to 230.6$ for (ii).

References

1. Kloeden P, Platen E, 1995. *Numerical Solution of Stochastic Differential Equations*, Springer, Heidelberg.
2. Roberts A J, 2015. *Model emergent dynamics in complex systems.* Section 20.4, SIAM, Philadelphia, isbn: 9781611973556.
3. Oksendal B, 2003, *Stochastic Differential Equations, An Introduction with Applications*, Springer, New York.
4. Van Kampen N G, 2007, *Stochastic Processes in Physics and Chemistry*, 3rd Edition, Elsevier North Holland.
5. Risken H. 1996 *The Fokker-Planck Equation*, Springer.
6. Dorodnitsyn A A. *Priklad Matm. i Mekhan*, **11**, 313-228 (1947) (in Russian), English Translation: (1953) *Trans. Am. Math. Soc*. **88**, pp. 1-24.
7. Peters R, Le Berre M, Pomeau Y. 2012 *Prediction of Catastrophes: An experimental Model*, Phys. Rev. **E 86**, 026207.
8. Hirsh M V, Smale S, Devaley R L, 2013, *Differential Equations, Dynamical Systems, and An Introduction to Chaos*, Academic Press, Amsterdan.
9. Jauslin HR. 1985 *A classification of Fokker-Planck models and the small and large noise asymptotics*, J Stat Phys **40** 147.
10. Tel T, Graham R, Hu G. 1989 *Nonequilibrium potentials and their power-series expansions*, Phys. Rev. **A 40**, 4065-4071.
11. Maier RS, Stein DL 1993 Phys. Rev. **E 48**, 931-938.
12. Rojas R., 2001 *Topicos en Física no lineal*, Tesis de Ingeniería Matematica, *Facultad de Ciencias Fisicas y Matematicas*, U. de Chile, Santiago.